



# An Alternatively Translated Isoform of *PPARG* Suggests AF-1 Domain Inhibition as an Insulin Sensitization Target

Xiaomi Du,<sup>1,2</sup> Karen Mendez-Lara,<sup>1</sup> Siqi Hu,<sup>1</sup> Rachel Diao,<sup>1</sup> Guru Bhavimani,<sup>1</sup> Ruben Hernandez,<sup>1</sup> Kimberly Glass,<sup>1</sup> Camila De Arruda Saldanha,<sup>1</sup> Jason Flannick,<sup>3,4</sup> Sven Heinz,<sup>1</sup> and Amit R. Majithia<sup>1</sup>

*Diabetes* 2025;74:651–663 | <https://doi.org/10.2337/db24-0497>

**Peroxisome proliferator-activated receptor  $\gamma$  (PPAR $\gamma$ ) is the pharmacologic target of thiazolidinediones, potent insulin sensitizers that prevent metabolic disease morbidity but are accompanied by adverse effects, such as weight gain, in part because of nonphysiologic transcriptional agonism. Using high-throughput genome engineering, we targeted nonsense mutations to every exon of *PPARG*, finding an ATG in exon 2 (chr3:12381414, CCDS2609 c.A403) that functions as an alternative translational start site. This downstream translation initiation site gives rise to a PPAR $\gamma$  protein isoform (M135), preferentially generated from alleles containing nonsense mutations upstream of c.A403. PPAR $\gamma$  M135 retains the DNA and ligand binding domains of full-length PPAR $\gamma$  but lacks the N-terminal activation function 1 (AF-1) domain. Despite being truncated, PPAR $\gamma$  M135 shows increased transactivation of target genes, but only in the presence of agonists. Accordingly, human missense mutations disrupting AF-1 domain function actually increase agonist-induced cellular PPAR $\gamma$  activity compared with wild type (WT), and carriers of these AF-1-disrupting variants are protected from metabolic syndrome. Therefore, we propose PPAR $\gamma$  M135 as a fully functional alternatively translated isoform that may be therapeutically generated to treat insulin resistance-related disorders.**

Insulin resistance is a major driver of the epidemic metabolic diseases that challenge global health (1). Thiazolidinediones (TZDs) comprise a class of drugs that decrease insulin resistance by agonizing proliferator-activated receptor  $\gamma$  (PPAR $\gamma$ ) (2), a nuclear hormone receptor that contains an autonomous activation function 1 (AF-1)

## ARTICLE HIGHLIGHTS

- Genetic screens were performed across *PPARG* to study how disruptive mutations across the full coding sequence affect function.
- An alternative translational start site in *PPARG* generates a truncated isoform, peroxisome proliferator-activated receptor  $\gamma$  (PPAR $\gamma$ ) M135, which lacks the N-terminal activation function 1 (AF-1) domain and shows increased agonist-induced transactivation of target genes.
- In human carriers of rare *PPARG* variants, AF-1 domain-disrupting genetic variants increase agonist-induced PPAR $\gamma$  activity and decrease metabolic syndrome severity.
- Targeting the AF-1 domain is a potential therapeutic strategy for insulin sensitization.

domain, DNA binding domain (DBD), and ligand binding domain (LBD) (Fig. 1A) (3). TZDs have demonstrated clinical efficacy in treating type 2 diabetes and cardiovascular disease (4), but their use has been limited by serious adverse effects, including weight gain and fluid retention (2). Much pharmacologic effort has focused on the development of selective PPAR $\gamma$  modulators that retain the benefits of TZDs without the attendant adverse effects, but successful compounds have not reached the clinic (5). Therefore, the need for alternative approaches to therapeutically activate PPAR $\gamma$  without PPAR-mediated adverse effects remains unmet.

Loss-of-function (LOF) mutations in *PPARG* occurring in the DBD and LBD have been shown to cause familial

<sup>1</sup>Division of Endocrinology and Metabolism, Department of Medicine, University of California San Diego, La Jolla, CA

<sup>2</sup>Bioinformatics and Systems Biology Graduate Program, University of California San Diego, La Jolla, CA

<sup>3</sup>Program in Medical and Population Genetics, Broad Institute of MIT and Harvard, Cambridge, MA

<sup>4</sup>Department of Pediatrics, Boston Children's Hospital, Boston, MA

Corresponding author: Amit R. Majithia, [amajithia@health.ucsd.edu](mailto:amajithia@health.ucsd.edu)

Received 15 June 2024 and accepted 21 January 2025

This article contains supplementary material online at <https://doi.org/10.2337/figshare.28255196>.

© 2025 by the American Diabetes Association. Readers may use this article as long as the work is properly cited, the use is educational and not for profit, and the work is not altered. More information is available at <https://www.diabetesjournals.org/journals/pages/license>.

partial lipodystrophy type 3 (FPLD3), a Mendelian genetic syndrome characterized by insulin resistance, metabolic syndrome, and gluteofemoral fat loss (6,7). These pathogenic FPLD3 mutations establish the clinical significance of the PPAR $\gamma$  DBD and LBD, but they represent only the tip of the iceberg in human protein-coding variants found in *PPARG* (8). In previous work, we identified hundreds of protein-coding variants in *PPARG* occurring in all protein domains, including the AF-1 domain (9). As with FPLD3, those that cause LOF in the DBD and LBD increase insulin resistance and type 2 diabetes risk. We observed no apparent clinical impact of LOF variants in the AF-1 domain, leaving in question its function in human metabolic health.

In this article, we report a novel protein isoform of PPAR $\gamma$  (PPAR $\gamma$  M135), which lacks the AF-1 domain and is generated from an alternative translational start site. Through biochemical and transcriptomic profiling, we found that PPAR $\gamma$  M135 demonstrated enhanced ligand-inducible transcriptional and functional activity compared with wild type (WT), leading us to a model of derepression by loss of AF-1. To evaluate the clinical consequence of this model, we identified and analyzed human carriers of *PPARG* variants that impair AF-1 function, finding that these variants increased PPAR $\gamma$  function and decreased metabolic syndrome severity in individuals who carry them. Taken together, our study findings propose AF-1 domain inhibition as a new targetable mechanism to activate PPAR $\gamma$ .

## RESEARCH DESIGN AND METHODS

### Cell Lines

Human monocytic leukemia cells (THP-1; TIB-202; American Type Culture Collection) and human preadipocyte cells (Simpson-Golabi-Behmel syndrome [SGBS]) were cultured, differentiated, and stimulated to activate PPAR $\gamma$  as described in the Supplementary Methods. Statistical analysis did not include sex, because all cells originated from the same male cell lines.

### Pooled Screens

Guide RNAs (sgRNAs) to target *PPARG* (Supplementary Table 1) were cloned into lentiCRISPRv2 (ID 52961; Addgene), and the vectors were pooled for virus production (2304; Mirus Bio). THP-1 cells were infected at a multiplicity of infection of 0.3, and edited cells were selected for using puromycin (P8833; Sigma-Aldrich). To assess the functional impact of *PPARG* insertions and deletions (indels), cells were differentiated, stimulated, and FACS sorted based on CD36 expression ( $n = 5$  independent sorts). Enrichment scores (ESs) were calculated as the log<sub>2</sub> ratio of CD36<sup>+</sup>/CD36<sup>-</sup> normalized counts. The impact of indels at each codon of *PPARG* was calculated based on previously published methods (9).

### PPARG Edited Cell Lines

The endonuclease Cas9 and guides Int-sgRNA, Ex1-sgRNA, Ex1-sgRNA2, and Ex3-sgRNA (Supplementary Table 3) were introduced into THP-1 and SGBS cells by lentiviral transduction. The transduced THP-1 cells were sorted at one cell per well into 96-well plates (BD FACSARIA II) and expanded. Infected SGBS cells were differentiated 7 days after infection as previously published (10). Genomic edits and zygosity were confirmed by Sanger sequencing.

### Western Blotting

Proteins were extracted, quantified, loaded into 4–12% Bis-Tris gels (NP0336; Invitrogen), and transferred onto 0.45- $\mu$ m nitrocellulose membranes (1620115; Bio-Rad Laboratories). Antibodies used were Cell Signaling Technology cat. nos. 2435 (PPAR $\gamma$  N-terminus), 2443 (PPAR $\gamma$  C-terminus), 43603 (cyclophilin B), 41185 (actin), 2920 (Akt), and 4060 (phospho-Akt Ser473), and fluorescent secondary antibodies used were cat. nos. 5366, 5151, and 5470. Imaging was performed on the Odyssey CLx imager (LI-COR).

### THP-1 Cells With Exogenous PPAR $\gamma$

To evaluate the complementation of PPAR $\gamma$  using WT and M135 PPAR $\gamma$  isoforms, in vitro transcription was performed as previously described (11) with the following primers: WT forward, 5'-GAATTTAATACGACTCACTATAAGGAAATACGCCACCATGGGTGAAACTCTGGGAGAT-3'; M135 forward, 5'-GAATTTAATACGACTCACTATAAGGAAATACGCCACCATGGCAATTGAATGTCGTGTCT-3'; and reverse, 5'-CTAGGACATCGCAGTCTGCACCTAGTACAAGTCCTTGTAGATCTCC-TG-3'.

The transcripts were electroporated into P $\gamma$ <sup>-/-</sup> THP-1 cells in a 4-mm cuvette with one 400-V 5-ms square wave pulse (Xcell; Bio-Rad Laboratories). To match PPAR $\gamma$  protein expression, 2  $\mu$ g M135 mRNA and 8  $\mu$ g WT mRNA were used for each electroporation of 3 million cells ( $n = 5$ ). Each sample was split into three aliquots for protein collection and differentiation with or without rosiglitazone treatment. RNA was extracted (R1050; Zymo Research) and sent for library preparation (Illumina Stranded mRNA Prep) and 100-bp paired-end sequencing (25 million reads per sample on the NovaSeq S4). Analysis was performed in R 4.1.3 using edgeR 3.36.0, limma v3.50.1, UpSetR v1.4.0, and fgsea v1.20.0 (12–15).

### SGBS Cells With Exogenous PPAR $\gamma$

*PPARG* cDNA was synthesized (Twist Bioscience) with synonymous mutations (CCDS2609 c.C594T, G603C, T610A, C611G) to eliminate the Ex3-sgRNA recognition sequence and PCR amplified to generate cDNA encoding PPAR $\gamma$ 2 and PPAR $\gamma$  M135. These sequences were cloned into doxycycline-inducible pCW (ID 184708; Addgene). Virus was produced, and SGBS P $\gamma$ <sup>-/-</sup> cells were infected to create the SGBS P $\gamma$ <sup>-/-</sup> + WT and SGBS P $\gamma$ <sup>-/-</sup> + M135 cell lines. Insulin stimulation was performed after 24-h serum starvation with 100 nmol/L insulin (I9278; Sigma-Aldrich).

## Human Genetics

For all exome-sequenced cohorts, variants within the genomic coordinates of *PPARG* (chr3: 12287368–12434356 hg38) were extracted, and variant annotation was performed using SnpEff v4.3 (16). Nomenclature used for missense variants is for the canonical *PPARG* transcript ENST00000287820.10; protein ENSP00000287820.6. Function scores were obtained from the *PPARG* saturation mutagenesis (9). Serum HDL cholesterol (field 30760), waist circumference (field 48), serum triglycerides (TG; field 30870), systolic blood pressure (SBP; field 4080), and glycated hemoglobin (HbA<sub>1c</sub>; field 30750) were extracted for all UK Biobank participants. SBP values were corrected for individuals reported to be taking blood pressure medication by adding 15 mm Hg (17), and TG values were log normalized. The TG to HDL (TG/HDL) ratio was log transformed and *z* normalized across UK Biobank. Regressions were adjusted for the covariates of age, age squared, sex, and the first 10 principal components of genetic ancestry.

## Data and Resource Availability

All biobank data used in this study are accessible through applications to the respective databases. Data and resources are available on request from the corresponding author.

## RESULTS

### Novel Functional PPAR $\gamma$ Isoform M135 Is Generated From an Alternative Translational Start Site

In our initial experiments, the endogenous *PPARG* locus was systematically disrupted by inducing indels in each coding *PPARG* exon in a human macrophage cell line (THP-1), a tractable model suitable for large-scale genetic perturbation that phenocopies *PPARG*-related transcriptional responses in adipocytes (9,18). Findings from THP-1s were confirmed and extended in human adipocytes models, the physiologically relevant cell type for metabolic disease. The effect of *PPARG* disruptions was measured by quantifying the ability of the resulting cells to transactivate CD36, a direct PPAR $\gamma$  transcriptional target (19). A custom lentiviral library of CRISPR/Cas9 constructs with sgRNAs targeting all coding exons, untranslated regions, and introns ( $n = 95$ ) (Supplementary Table 1) was introduced into THP-1 monocytes at one construct per cell. The resulting population of genome-edited cells was differentiated into macrophages, stimulated with 1  $\mu$ mol/L PPAR $\gamma$  agonist rosiglitazone, and sorted by FACS according to the expression of CD36 (Fig. 1B). The CD36<sup>+</sup> and CD36<sup>−</sup> populations were sequenced to recover the identities of the sgRNAs, and an enrichment score (ES) was calculated based on the counts of each sgRNA in the CD36<sup>+</sup>/CD36<sup>−</sup> pools (Fig. 1B). Intron-targeting sgRNAs introduced as controls had an ES of  $0.487 \pm 0.025$ . As expected, targeting sgRNAs to exon B of *PPARG*, specific to the PPAR $\gamma$ 2 isoform, did not reduce CD36 activity (ES  $0.622 \pm 0.035$ ), and most sgRNAs targeted to exons downstream of the PPAR $\gamma$ 1 start site caused severe loss of CD36

transactivation (ES  $-1.33 \pm 0.147$ ). Intriguingly, five sgRNAs targeting exon 1 of *PPARG*, downstream of the PPAR $\gamma$ 1 start site, which would be predicted to maximally disrupt the protein sequence, had little effect on CD36 transactivation (ES  $0.597 \pm 0.084$ ), suggesting an intact PPAR $\gamma$  response in the cells that harbored them (Fig. 1C).

To further understand this unexpected finding, we analyzed data generated from a previously conducted saturation mutagenesis study of *PPARG* that contained indels at every codon of the PPAR $\gamma$ 2 cDNA (CCDS2609) and calculated function scores (FSs) such that WT *PPARG* had an FS of 0 (Supplementary Table 2) (9). Most indels that caused frameshift terminations in *PPARG* completely inhibited CD36 transactivation, as shown by negative FSs. However, frameshifting indels in the 5' region of the cDNA, predicted to cause early termination of protein translation, paradoxically retained cellular PPAR $\gamma$  transactivation (FS  $0.0322 \pm 0.0186$ ). This concurred with our finding of tolerated exon 1 disruptions at the endogenous *PPARG* locus (Fig. 1C) and suggested a possible postsplicing mechanism for retained PPAR $\gamma$  activity. The tolerance to early frameshifting indels was observed until c.A403, after which frameshifting indels induced significant dysfunction (FS  $-1.16 \pm 0.0074$ ). These findings were replicated in experiments using prostaglandin J2, a putatively endogenous PPAR $\gamma$  ligand (9) (Supplementary Fig. 1A). C.A403-405 encodes a methionine, leading us to hypothesize an alternative translation initiation site, which would explain the preservation of PPAR $\gamma$  transactivation functions in transcripts with frameshift and nonsense-inducing indels before c.A403.

A translation initiation site at CCDS2609 c.A403 (hg38:chr3:12381414; ENSP00000287820 p.M135) would lead to a protein isoform (PPAR $\gamma$  M135) shorter than PPAR $\gamma$ 2 by 134 amino acids with a predicted molecular weight of  $\sim 40$  kDa. To evaluate this hypothesis, we engineered clonal THP-1 monocytes with disruptions in exon 1, exon 3, and a *PPARG* intron using CRISPR/Cas9 (Ex1-sgRNA chr3:12379745, Ex3-sgRNA chr3:12392733, Int-sgRNA chr3:12363492) (Fig. 1A). Two independent cell lines were derived for each of the following genotypes: Int-sgRNA<sup>+/+</sup>, Ex1-sgRNA<sup>+/-</sup>, Ex1-sgRNA<sup>-/-</sup>, and Ex3-sgRNA<sup>-/-</sup> (Supplementary Table 3). Immunoblotting with PPAR $\gamma$  antibodies targeting N-terminal (p.Asp69) and C-terminal (p.His494) epitopes was performed on differentiated THP-1s. The N-terminal blot showed a 53-kDa band for full-length PPAR $\gamma$ 1 in control (Int-sgRNA) and heterozygous Ex1-sgRNA samples, whereas no PPAR $\gamma$  bands were detected in homozygous Ex1-sgRNA or Ex3-sgRNA cells (Fig. 1E). The C-terminal PPAR $\gamma$  blot corroborated the PPAR $\gamma$ 1 detection and identified a band of  $\sim 40$  kDa in Ex1-sgRNA cells, matching the predicted size of PPAR $\gamma$  M135, with higher intensity in Ex1-sgRNA<sup>-/-</sup> cells (Fig. 1F). Additional smaller bands may reflect alternative translation initiation sites upstream of p.M135. No PPAR $\gamma$  protein was detected in Ex3-sgRNA<sup>-/-</sup> cells, indicating complete loss of PPAR $\gamma$  (Fig. 1F).

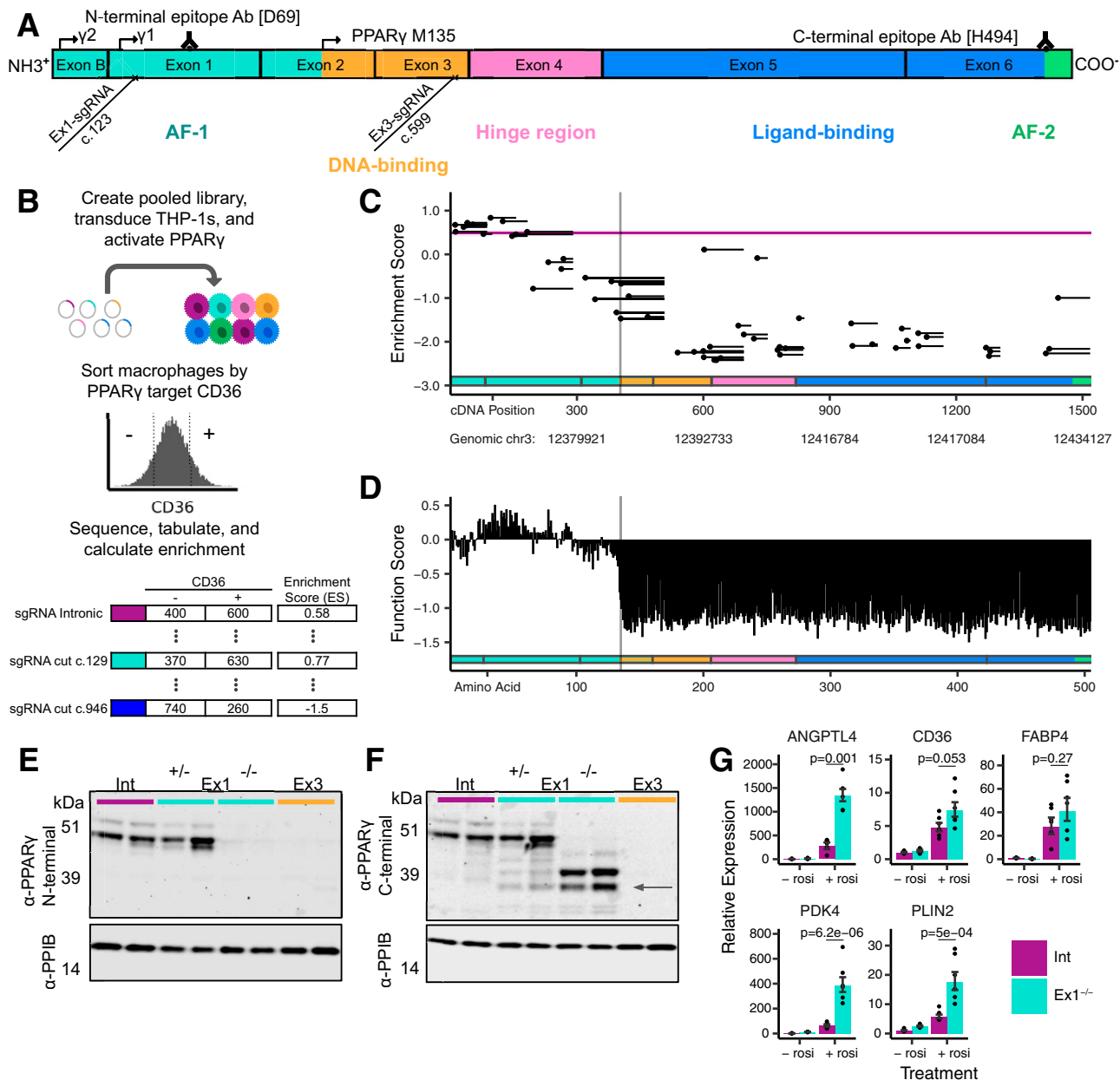


**Figure 1**—Functional screens across *PPARG* reveal an alternative translational start site at p.M135. **A**: Linear representation of PPAR $\gamma$  indicating start sites for  $\gamma_1$ ,  $\gamma_2$ , and novel M135. Guides and cut sites (Ex1-sgRNA; chr3:12379745 and Ex3-sgRNA; chr3:12392733, hg38) of CRISPR/Cas9 monoclonal generated cells are shown. Domain structure of PPAR $\gamma$  protein is represented in color, and epitopes of N-terminus and C-terminus antibodies (Abs) are indicated. **B**: A library of 95 sgRNAs targeting *PPARG* was generated and transduced into THP-1 monocytes, such that each cell received a single construct. Polyclonal THP-1s were differentiated into macrophages, stimulated with PPAR $\gamma$  agonist, 1  $\mu$ M rosiglitazone (rosi), and sorted by FACS for expression of PPAR $\gamma$  target CD36 into bins of low (–) and high (+) PPAR $\gamma$  activity ( $n = 5$  independent replicate sorts). **C**: Enrichment scores (ESs) from the CRISPR screen across *PPARG*. Mean ES for each guide across five sort replicates is plotted along *PPARG2* cDNA based on its cut site (dot) and predicted termination after one-base indel (line). Horizontal purple line indicates mean and SE of intronic guides ( $n = 18$ ). PPAR $\gamma$  p.M135 is denoted by vertical line. **D**: Function scores (FSs) of indels at each amino acid of PPAR $\gamma_2$  calculated as previously published (9). FS = 0 refers to WT activity. **E** and **F**: Western blots against N-terminus (**E**) and C-terminus (**F**) of PPAR $\gamma$  protein were performed to detect PPAR $\gamma$  isoforms from monoclonal cell lines, showing that pre-M135–edited cell lines (Ex1) generate truncated PPAR $\gamma$  bands, including predicted p.M135 at 40 kDa (arrow), as opposed to post-M135 (Ex3) targeted cell lines and intronic cell lines (Int). **G**: Relative expression of PPAR $\gamma$  target genes in *PPARG*–targeted monoclonal cell lines, with or without rosi treatment, with GAPDH as housekeeping gene and Int-sgRNA–edited cells with 0 rosi as control. In response to rosi, increases in *ANGPTL4*, *PDK4*, and *PLIN2* for Ex1–edited cells ( $n = 6$ ; cyan) were greater than increases in Int–edited cells ( $n = 6$ ; purple); Welch two-sample  $t$  test on  $\Delta$  Ct values. Nonsignificant increases in *CD36* and *FABP4* were also observed in Ex1–edited cells.

To compare the transcriptional profiles of cells expressing WT and PPAR $\gamma$  M135, the Int-sgRNA<sup>+/+</sup> and Ex1-sgRNA<sup>-/-</sup> clonal cell lines were differentiated into macrophages, stimulated with 1  $\mu$ mol/L rosiglitazone and assessed for gene expression at several canonical PPAR $\gamma$  target genes (Fig. 1G). On agonist induction, the Ex1-sgRNA<sup>-/-</sup> cells expressed significantly higher levels of *ANGPTL4* (20) ( $P = 0.001$ ), *PDK4* (21) ( $P = 6.2e-6$ ), and *PLIN2* (22) ( $P = 5e-4$ ) than the Int-sgRNA<sup>+/+</sup> cells. These PPAR $\gamma$  M135-expressing cells also showed nonsignificant increases in *CD36* and *FABP4* expression. Because PPAR $\gamma$  plays a role in monocyte-to-macrophage differentiation, we measured *ITGAM* (CD11b) (23) and *CD68* (24) to assess phorbol 12-myristate 13-acetate (PMA)-induced differentiation as a potential confounder. After PMA treatment, CD11b and *CD68* expression increased similarly in Ex1-sgRNA<sup>-/-</sup> and Int-sgRNA<sup>+/+</sup> cells (Supplementary Fig. 1B).

We subsequently isolated and compared the transactivation potentials of WT and PPAR $\gamma$  M135. A PPRE-driven luciferase reporter (25) and WT PPAR $\gamma$  or PPAR $\gamma$  M135 mRNA were transfected into HEK293s, which have minimal endogenous PPAR $\gamma$  activity (26). In this system, PPAR $\gamma$  M135 activated transcriptional activity more potently than WT when induced with rosiglitazone (Supplementary Fig. 1C). We further compared the stability of PPAR $\gamma$  M135 with that of WT by performing a cycloheximide chase (27) in the heterozygous Ex1-sgRNA cells that generate both isoforms (Supplementary Fig. 1D). The M135 isoform degraded more slowly than PPAR $\gamma$ 1 (Supplementary Fig. 1E), which could contribute to its enhanced transactivation potential.

### Ligand-Activated PPAR $\gamma$ M135 Transactivates Target Genes More Potently Than WT PPAR $\gamma$ in THP-1s

We next sought to isolate the activity of PPAR $\gamma$  M135 and evaluate its effect on global transcriptional profiles in comparison with full-length WT PPAR $\gamma$ . To compare the direct transcriptional responses of M135 and WT, we performed RNA sequencing on PPAR $\gamma$ -null (P $\gamma$ <sup>-/-</sup>) THP-1 monocytes electroporated with in vitro-transcribed mRNA of each of the two PPAR $\gamma$  isoforms; EGFP mRNA was also electroporated as a process control. In preliminary experiments, mRNA amounts for each isoform were titrated to express similar amounts of protein at the point of harvest (Supplementary Fig. 2A and B), such that 2  $\mu$ g PPAR $\gamma$  M135 mRNA and 8  $\mu$ g PPAR $\gamma$  WT were used for each electroporation. The electroporated cells were differentiated into macrophages to mimic the cellular context in which PPAR $\gamma$  is active (28) and treated with 0 (-) and 1  $\mu$ mol/L (+) rosiglitazone. As a positive control, WT (P $\gamma$ <sup>+/+</sup>) THP-1 cells with intact *PPARG* were also treated with or without rosiglitazone and transcriptionally profiled (Fig. 2A).

After filtering for low expression, 16,732 transcripts were retained for analysis across all samples. As expected, rosiglitazone treatment increased gene expression of canonical PPAR $\gamma$  target genes, including *CD36*, *FABP4* (3), and *PLIN2* (22) (Fig. 2B). Remarkably, PPAR $\gamma$  M135-electroporated

(P $\gamma$ <sup>-/-</sup> + M135) cells exhibited greater agonist-induced transcriptional responses for some of these targets compared with P $\gamma$ <sup>-/-</sup> + WT or P $\gamma$ <sup>+/+</sup> THP-1 macrophages, despite comparable PPAR $\gamma$  protein levels (log2 fold change [log2FC]: *CD36*: P $\gamma$ <sup>-/-</sup> + M135 4.22, P $\gamma$ <sup>+/+</sup> 2.94, and P $\gamma$ <sup>-/-</sup> + WT 1.62; *PLIN2*: P $\gamma$ <sup>-/-</sup> + M135 3.35, P $\gamma$ <sup>+/+</sup> 3.24, and P $\gamma$ <sup>-/-</sup> + WT 1.50).

To comprehensively evaluate if M135 generated a stronger agonist-induced transcriptional response than WT in P $\gamma$ <sup>-/-</sup> cells, we performed a series of differential expression analyses. We first identified the top-ranked PPAR $\gamma$  target genes, defined as the 50 most significant differentially expressed genes (DEGs) in P $\gamma$ <sup>+/+</sup> cells with or without rosiglitazone, and then compared the log2FC of the same genes across P $\gamma$ <sup>-/-</sup> + WT and P $\gamma$ <sup>-/-</sup> + M135 with or without rosiglitazone (Fig. 2C). Of the top 50 P $\gamma$ <sup>+/+</sup> DEGs, 46 were also differentially expressed in P $\gamma$ <sup>-/-</sup> + M135 ( $P < 0.05$  [same sign log2FC]), whereas only 33 were differentially expressed in P $\gamma$ <sup>-/-</sup> + WT. Moreover, in several key genes, including *PDK4*, *DYSF*, *ANGPTL4*, *ALOX5AP*, and *CYBB* (29–31), P $\gamma$ <sup>-/-</sup> + M135 had a greater activation or repression than P $\gamma$ <sup>+/+</sup> cells (Fig. 2C), despite transient and lower PPAR $\gamma$  protein expression per cell (Supplementary Fig. 2A and B). Across all the P $\gamma$ <sup>+/+</sup> DEGs ( $n = 1,779$ ), the magnitude of gene expression change was more similar for P $\gamma$ <sup>-/-</sup> + M135 cells (slope 0.85) than for P $\gamma$ <sup>-/-</sup> + WT cells (slope 0.36), indicating greater potency of M135 in mediating agonist-induced PPAR $\gamma$  gene expression response than WT (Fig. 2D).

We then queried for DEGs specific to PPAR $\gamma$  M135 to assess if the lack of AF-1 domain in M135 resulted in transactivation/repression of genes not regulated by WT PPAR $\gamma$ . In response to rosiglitazone treatment, P $\gamma$ <sup>-/-</sup> + M135 had the greatest number of DEGs ( $n = 4,247$ ) (Fig. 2E), as compared with P $\gamma$ <sup>-/-</sup> + WT ( $n = 1,794$ ) or P $\gamma$ <sup>+/+</sup> ( $n = 1,779$ ). Of the 4,247 DEGs, 2,313 were exclusive to P $\gamma$ <sup>-/-</sup> + M135 (Fig. 2E). To understand the gene expression programs captured by these putative M135-specific genes, we performed gene set overrepresentation analysis (32,33) among the Gene Ontology Biological Process pathways (34,35) and found 28 overrepresented pathways that were confirmed to have been altered by rosiglitazone treatment in M135-complemented cells ( $P < 0.05$ ) (Supplementary Table 4). Among these, 21 of 28 were similarly altered, although to a lesser degree, by rosiglitazone treatment in either WT-electroporated cells or P $\gamma$ <sup>+/+</sup> THP-1s (Fig. 2F). Taken together, these analyses suggest that PPAR $\gamma$  M135 regulates similar gene expression programs as WT, but more potently when induced by rosiglitazone, perhaps because of derepression from the loss of the N-terminal AF-1 domain (36).

### Human Preadipocytes Generate PPAR $\gamma$ M135 and More Potently Upregulate Target Genes Than WT

Because many of the major metabolic effects of *PPARG* on human physiology occur in adipocytes (8), we evaluated

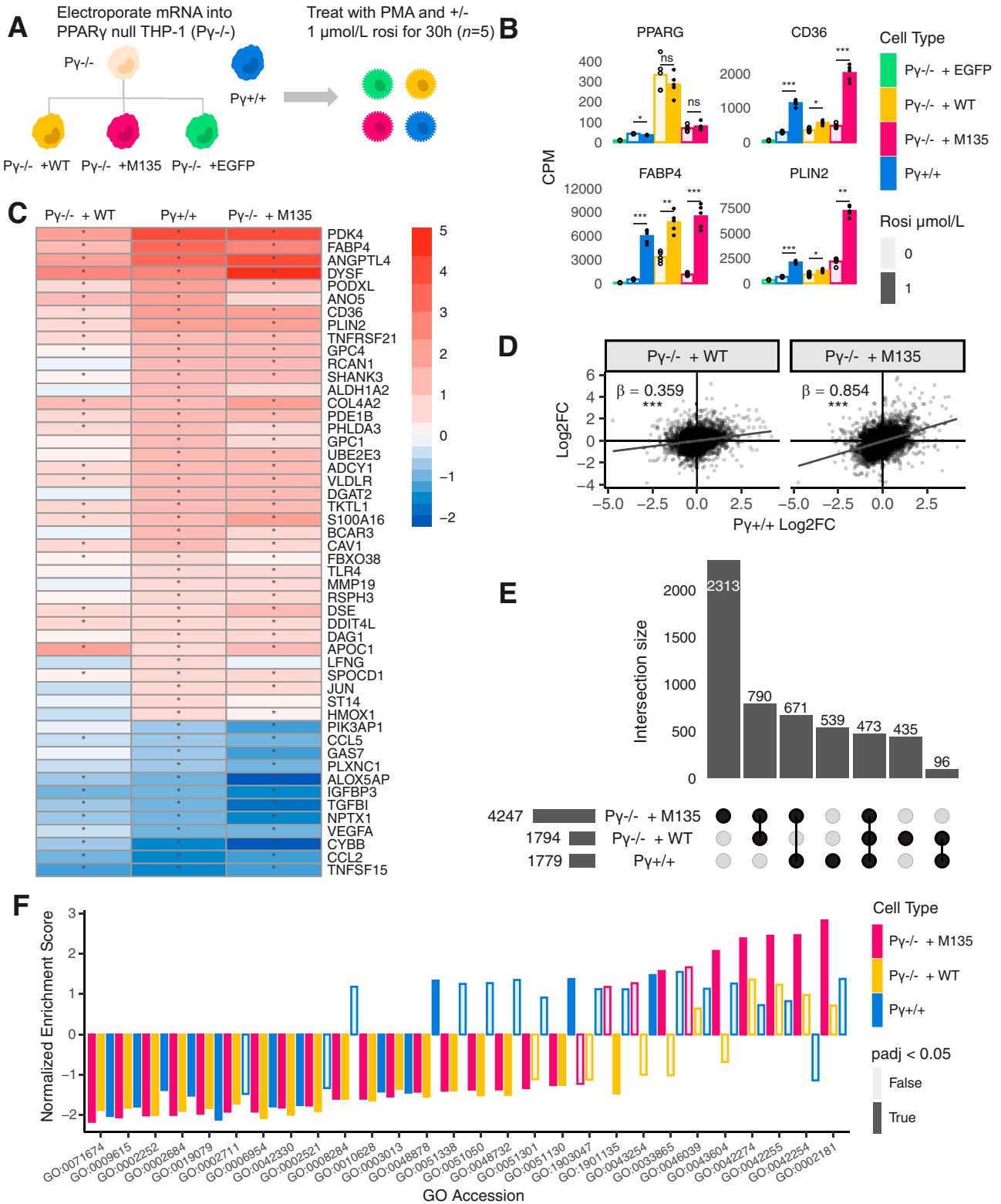


**Figure 2**—PPAR $\gamma$  M135 more potently activates ligand-stimulated gene expression as compared with WT. **A**: PPAR $\gamma$  WT and M135 mRNAs, along with control EGFP mRNA, were generated through in vitro transcription and electroporated into PPAR $\gamma$ -null (P $\gamma$ <sup>-/-</sup>) THP-1 monocytes. Electroporated cells and WT THP-1s (P $\gamma$ <sup>+/+</sup>) were differentiated into macrophages and treated with or without 1  $\mu$ mol/L rosiglitazone (rosi) for 30 h before protein and RNA were collected (n = 5 per condition). **B**: RNA sequencing expression in counts per million (CPM) of PPARG and selected PPAR $\gamma$  target genes. In response to rosi treatment, P $\gamma$ <sup>-/-</sup> + M135 activates CD36 and PLIN2 with greater fold change than P $\gamma$ <sup>-/-</sup> + WT or P $\gamma$ <sup>+/+</sup>. **C**: Heat map of log<sub>2</sub>FC in response to rosi for each cell type of top 50 DEGs in P $\gamma$ <sup>+/+</sup> THP-1s, as ranked by P value. Asterisks indicate DEGs changing in same direction with Benjamin-Hochberg-corrected P < 0.05. **D**: Scatterplot of all 1,779 P $\gamma$ <sup>+/+</sup> DEG log<sub>2</sub>FC values, comparing log<sub>2</sub>FC in P $\gamma$ <sup>+/+</sup> with log<sub>2</sub>FC in P $\gamma$ <sup>-/-</sup> + WT and P $\gamma$ <sup>-/-</sup> + M135. Regression slopes ( $\beta$ ) are significant for both,

whether adipocytes could also generate PPAR $\gamma$  M135 and to what functional consequence. We targeted a human preadipocyte cell line (SGBS (37)) with disruptions in exon 1, exon 3, and a *PPARG* intron (Ex1-sgRNA2 cut site at hg38 chr3:12379716, Ex3-sgRNA chr3:12392733, and Int-sgRNA chr3:12363492) (Fig. 3A and Supplementary Table 3). The edited cells were treated with inducers of adipocyte differentiation and examined for PPAR $\gamma$  protein expression, target gene expression, and adipocyte differentiation efficiency. After 4 days of differentiation, we were able to detect both PPAR $\gamma$  WT and M135 in exon 1–targeted cells, whereas exon 3–targeted cells expressed no PPAR $\gamma$ , and control cells expressed only WT PPAR $\gamma$  (Fig. 3B and C). These results indicated that like THP-1 macrophages, SGBS adipocytes are capable of alternatively generating PPAR $\gamma$  M135 in response to disruptive mutations targeted to exon 1.

To evaluate the ability of preadipocytes expressing PPAR $\gamma$  M135 to activate PPAR $\gamma$  target genes, we queried the gene expression of several targets during early adipocyte differentiation (Fig. 3D). SGBS preadipocytes that expressed PPAR $\gamma$  M135 increased expression of *CD36* ( $P = 0.022$ ) and *PDK4* ( $P = 5.2e-5$ ) to a significantly greater extent than PPAR $\gamma$  WT–expressing cells, similar to macrophages (Fig. 1G) and showed a trend toward increased expression of *FABP4* ( $P = 0.22$ ). Furthermore, we examined adiponectin (*ADIPOQ*), an adipokine and PPAR $\gamma$  target specific to adipocytes (38), and found it also to be significantly upregulated by PPAR $\gamma$  M135 expressing–adipocytes ( $P = 0.017$ ) compared with WT (Fig. 3D). Cells targeted at exon 3, which expressed no PPAR $\gamma$ , did not upregulate the expression of any of these genes.

Finally, we characterized the ability of PPAR $\gamma$  M135–expressing SGBS cells to mature into adipocytes and accumulate lipids during differentiation (Fig. 3E and F). Exon 1–targeted PPAR $\gamma$  M135–expressing SGBS cells differentiated and accumulated lipids at the same rate as control PPAR $\gamma$  WT–expressing cells ( $P = 0.933$ ), whereas exon 3–targeted cells had significantly reduced lipid accumulation ( $P = 2e-16$ ). These analyses show that like macrophages, human preadipocytes can generate the PPAR $\gamma$  M135 isoform, and the truncated isoform is fully functional in driving differentiation into mature, lipid-laden adipocytes.

### PPAR $\gamma$ M135 Enhances Adipocyte Insulin Response Compared With WT

To isolate the effect of PPAR $\gamma$  M135, we transduced P $\gamma$ <sup>-/-</sup> SGBS cells (i.e., Ex3-sgRNA targeted cells) with

doxycycline-inducible WT PPAR $\gamma$ 2 cDNA (SGBS P $\gamma$ <sup>-/-</sup> + WT) or PPAR $\gamma$  M135 cDNA (SGBS P $\gamma$ <sup>-/-</sup> + M135) transgenes and evaluated differentiation/lipid accumulation and insulin response (Fig. 4A). These cells only express PPAR $\gamma$  (WT or M135) when treated with doxycycline (Fig. 4B) and differentiate to a similar degree only when PPAR $\gamma$  is induced ( $P = 0.56$ ) (Fig. 4C and D).

To assess insulin response, control (intronic), SGBS P $\gamma$ <sup>-/-</sup> + WT, and SGBS P $\gamma$ <sup>-/-</sup> + M135 cells were differentiated, stimulated with insulin, and immunoblotted for phosphorylated Akt (S473) and total Akt. In response to insulin, all cell lines phosphorylated Akt, and the response was augmented in doxycycline-treated SGBS P $\gamma$ <sup>-/-</sup> + WT and SGBS P $\gamma$ <sup>-/-</sup> + M135 (ANOVA  $P = 1.33e-13$ ; Tukey honest significant difference [HSD]  $P = 3.67e-8$  for WT and  $P = 3.43e-11$  for M135) (Fig. 4E and F). Notably, PPAR $\gamma$  M135–expressing adipocytes showed increased insulin-stimulated Akt phosphorylation compared with both WT ( $P = 0.025$ ) and control SGBS ( $P = 0.045$ ), indicating an enhanced insulin response.

### Missense Mutations That Impair AF-1 Function Increase PPAR $\gamma$ Transactivation and May Protect Against Metabolic Syndrome in Human Carriers

Next, we sought to evaluate the potential in vivo consequence of nonsense mutations in the *PPARG* sequence before chr3:12381414 by identifying human carriers of such mutations and performing genotype:phenotype correlation under the hypothesis that carriers would not exhibit insulin resistance given the enhanced molecular activity of PPAR $\gamma$  M135 resulting from AF-1 domain deletion. Across biobanks and databases comprising >1.2 million individuals with sequencing at the *PPARG* locus, we found only seven carriers of nonsense mutations before chr3:12381414 (Supplementary Table 5). Among these, two had no evidence of metabolic syndrome or insulin resistance past 50 years of age, one had type 2 diabetes but no ascertainment of insulin resistance or metabolic syndrome, and four had no available phenotypic information.

Because the number of human pre-M135 nonsense mutation carriers was insufficient to make robust inferences, we turned to carriers of *PPARG* missense variants to test the hypothesis that genetic variants abrogating AF-1 domain function would enhance PPAR $\gamma$  activity and thereby increase insulin sensitivity in vivo (Fig. 5A). Although missense variants are not equal to having the M135 isoform, they can model how disruptions to the AF-1 domain affect PPAR $\gamma$  activity in vivo. We rationalized this hypothesis based on recent data showing that

but P $\gamma$ <sup>-/-</sup> + M135 transcriptional response more closely recapitulates P $\gamma$ <sup>+/+</sup>. *E*: Upset plot of DEGs per cell type with or without rosi. Left horizontal bars show total DEGs for each condition. Filled circles connected by lines indicate intersections among the three conditions, and vertical bars show number of DEGs in corresponding intersections. *F*: Normalized ESs in the Gene Ontology (GO) Biological Process pathways for P $\gamma$ <sup>-/-</sup> M135–specific genes. Overall transcriptional pathway activation by P $\gamma$ <sup>+/+</sup>, P $\gamma$ <sup>-/-</sup> + WT, and P $\gamma$ <sup>-/-</sup> + M135 are similar and consistent. Pathway names for GO IDs are listed in Supplementary Table 4. \*Benjamini-Hochberg–corrected (BH)  $P < 0.01$ , \*\*BH  $P < 1e-4$ , \*\*\*BH  $P < 1e-8$  (B) and \*\*\* $P < 2e-16$  (D). adj, adjusted; ns, not significant.

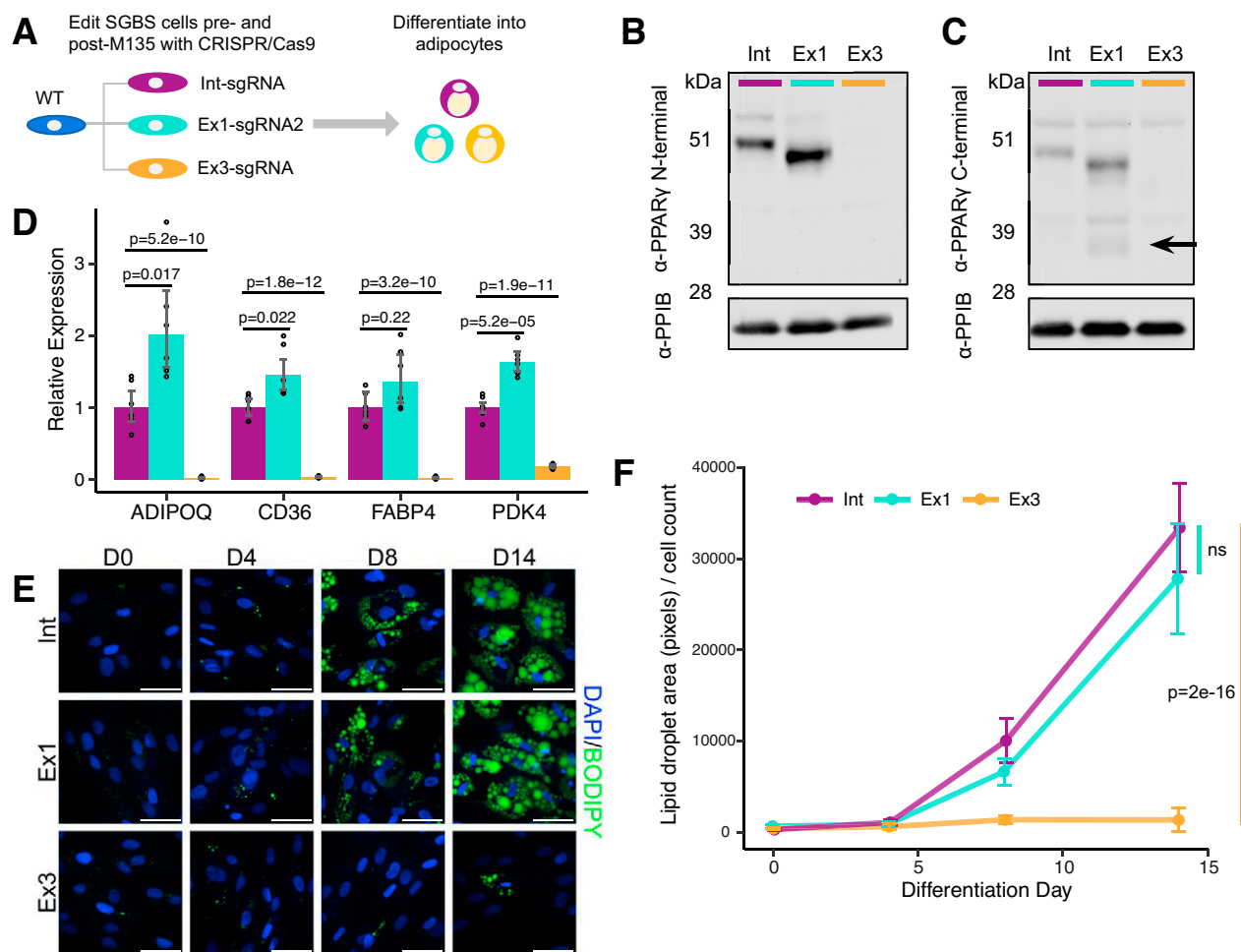


**Figure 3**—Human preadipocytes generate PPAR $\gamma$  M135 and more potently upregulate target genes than WT. **A:** SGBS cells were transduced with a vector containing Cas9 and a sgRNA targeting *PPARG* exon 1 (chr3:12379716), exon 3 (chr3:12392733), or intron (chr3:12363492). Preadipocytes were differentiated into adipocytes. **B** and **C:** Western blot for N-terminus (**B**) and C-terminus (**C**) of PPAR $\gamma$  in SGBS preadipocytes treated with *PPARG*-targeting constructs (**A**) at 4 days post-differentiation. Ex1-targeted preadipocytes generate PPAR $\gamma$  M135 at 40 kDa (arrow), whereas Ex3-targeted cells do not express any PPAR $\gamma$ . Ex1-targeted cells also express band  $\sim$ 50 kDa, consistent with translation initiation at PPAR $\gamma$  p.M53. **D:** Expression of PPAR $\gamma$  target genes at 4 days of differentiation by quantitative PCR. Ex1-targeted cells expressed higher levels of *ADIPOQ*, *CD36*, and *PDK4* compared with control. Ex3-edited cells minimally express all PPAR $\gamma$  target genes ( $n = 6$  replicates per sample;  $P$  values from linear models of  $\Delta$  Ct; see Supplementary Methods for more details). **E** and **F:** Differentiation time course for Int-, Ex1-, and Ex3-targeted SGBS cells at days 0, 4, 8, and 14. Cells were fixed and stored in PBS on their respective collection dates, stained on day 14 for nuclei (DAPI; blue) and lipids (BODIPY; green), and imaged. **E:** Imaged at 40 $\times$  magnification. Ex1 SGBS cells differentiate in par with Int, and Ex3 SGBS cells do not accumulate lipids. Scale bar, 50  $\mu$ m. **F:** Quantification of lipid accumulation in SGBS cells. Data were log normalized and regressed against genotype and differentiation day to determine effect of genotype. Ex1 was not different from Int ( $P = 0.933$ ), and Ex3 resulted in a significantly different pace ( $P = 2e-16$ ).

the AF-1 domain intramolecularly binds to the LBD of PPAR $\gamma$ , and this interaction inhibits ligand-dependent activity (36). We identified all carriers of rare (minor allele frequency  $<0.001$ ) protein-coding variants in *PPARG* in the UK Biobank ( $n = 454,787$ ) (39) and analyzed the cellular function and amino acid position of the variants carried in relation to the insulin sensitivity-related phenotypes of the individuals carrying them. To quantify PPAR $\gamma$  activity, we leveraged the PPAR $\gamma$  FS derived from our previously published deep mutational scan (9), in which every possible missense variant was scored by its transactivation of CD36 (9). We found 1,250 carriers of 260 unique rare, protein-coding *PPARG* variants and partitioned them by

pre-/post-M135 and by the BLOSUM62 substitution matrix, which quantifies the tolerance of amino acids to substitution across evolutionary distance (40). Variants were categorized as conservative (BLOSUM62  $>0$ ) or nonconservative (BLOSUM62  $<0$ ). Nonconservative substitutions in AF-1 (median FS 2.21) had higher PPAR $\gamma$  FSs than conservative substitutions (median FS 1.56), whereas nonconservative substitutions post-M135 in the DBD and LBD (median FS  $-0.158$ ) showed decreased PPAR $\gamma$  FSs relative to conservative mutations (median FS  $-0.376$ ; ANOVA  $P < 2e-16$ ; adjusted  $P < 0.005$  for each pairwise comparison by Tukey HSD) (Fig. 5B). These data support the hypothesis that missense variants disrupting AF-1

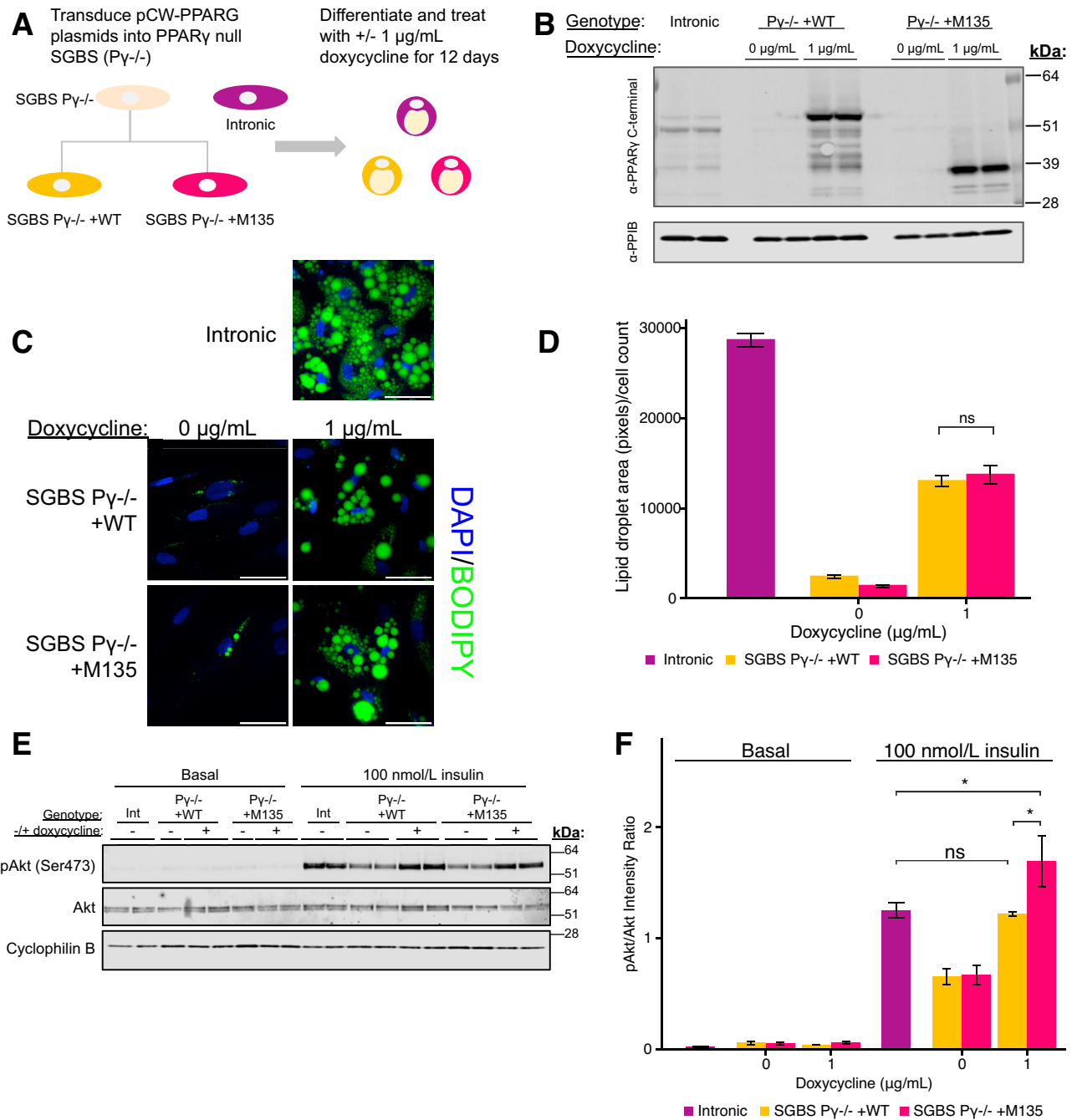


**Figure 4**—PPAR $\gamma$  M135 enhances adipocyte insulin response compared with WT. **A**: SGBS P $\gamma$ <sup>-/-</sup> cells were transduced with doxycycline-inducible vectors expressing PPARG WT and M135. Preadipocytes were differentiated and treated with or without doxycycline. **B**: PPAR $\gamma$  expression in SGBS cells. SGBS P $\gamma$ <sup>-/-</sup> cells with PPARG transgenes only express PPAR $\gamma$  when treated with doxycycline. **C** and **D**: Intronic, SGBS P $\gamma$ <sup>-/-</sup> + WT, and SGBS P $\gamma$ <sup>-/-</sup> + M135 cells were differentiated for 12 days, fixed, stained for nuclei (DAPI; blue) and lipid accumulation (BODIPY; green), and imaged. **C**: Imaged at 40 $\times$  magnification. PPAR $\gamma$  M135 is sufficient to induce differentiation and lipid uptake in SGBS P $\gamma$ <sup>-/-</sup> cells. Scale bar, 50  $\mu$ m. **D**: Quantification of lipid accumulation. SGBS P $\gamma$ <sup>-/-</sup> + M135 cells accumulate same amount of lipids as SGBS P $\gamma$ <sup>-/-</sup> + WT ( $n = 12$  images per well, 4 wells per genotype;  $t$  test  $P = 0.56$ ). **E** and **F**: Intronic, SGBS P $\gamma$ <sup>-/-</sup> + WT, and SGBS P $\gamma$ <sup>-/-</sup> + M135 cells were treated with or without doxycycline, with or without 100 nmol/L insulin, for 20 min and immunoblotted for phosphorylated Akt (pAkt) and total Akt ( $n = 4$  biological replicates). **E**: Representative immunoblot. **F**: pAkt/Akt intensity ratios were significantly different across conditions (ANOVA  $P = 1.33e-13$ ). Pairwise comparisons are highlighted between 100 nmol/L insulin-stimulated samples for SGBS P $\gamma$ <sup>-/-</sup> + M135 and SGBS P $\gamma$ <sup>-/-</sup> + WT cells treated with 1  $\mu$ g/mL doxycycline (Tukey HSD  $*P = 0.025$ ), SGBS P $\gamma$ <sup>-/-</sup> + M135 + doxycycline and Intronic (Tukey HSD  $*P = 0.045$ ), and SGBS P $\gamma$ <sup>-/-</sup> + WT + doxycycline and Intronic ( $P = 0.99$  [not significant (ns)]).

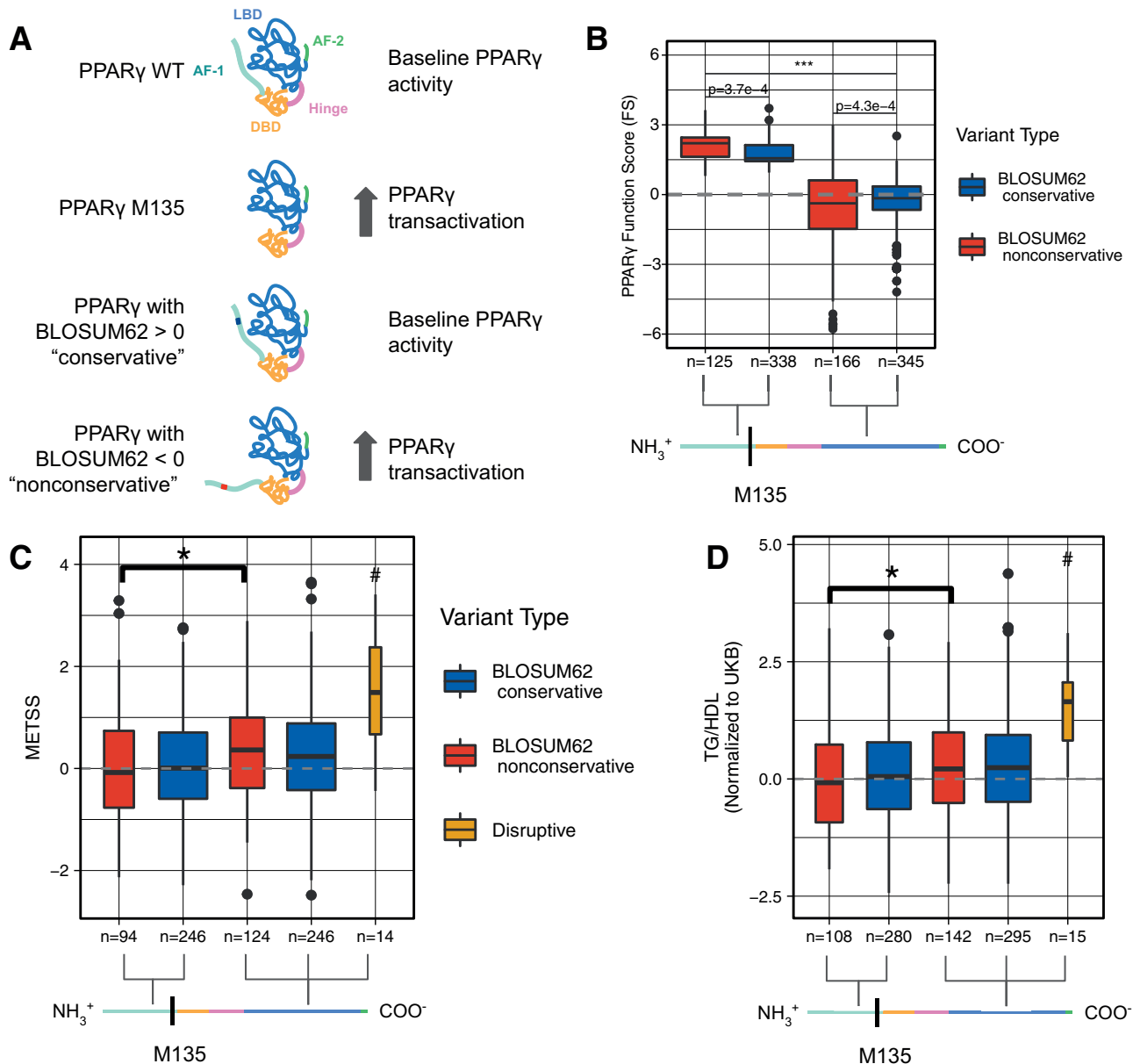


**Figure 5**—Human carriers of variants in PPAR $\gamma$  that impair AF-1 domain are protected from metabolic dysfunction. **A**: Representation of AF-1 hypothesis. Removing or having evolutionarily nonconserved amino acid substitutions in AF-1 domain prevents/impairs binding of AF-1 to LBD, thereby increasing transcriptional activity (AF-1 cyan; DBD orange; hinge pink; LBD blue; AF-2 green). Protein representation modeled after PPAR $\gamma$  crystal structure shown in Mosure et al. (36). **B**: FSs for *PPARG* missense variants (minor allele frequency <0.001) from UK Biobank (UKB;  $n = 454,787$ ) by position (i.e., pre-/post-M135) and evolutionary conservation (conservative BLOSUM62 <0; nonconservative BLOSUM62 >0) category. Pre-M135 nonconservative variants ( $n = 125$  carriers) have highest FSs (median FS 2.21), followed by pre-M135 conservative ( $n = 338$ ; median FS 1.56), post-M135 conservative ( $n = 345$ ; median FS -0.158), and post-M135 nonconservative ( $n = 166$ ; median FS -0.376). All pairwise comparisons between categories are significant by ANOVA and Tukey HSD. **C**: METSS by position and conservation, as in **B**. Carriers of pre-M135 nonconservative missense variants ( $n = 94$ ; median METSS -0.079) have lower METSSs than carriers of pre-M135 conservative missense variants ( $n = 246$ ; median METSS 0.006), followed by carriers of post-M135 conservative missense variants ( $n = 246$ ; median METSS 0.24) and carriers of post-M135 nonconservative missense variants ( $n = 124$ ; median METSS 0.36). Disruptive variants (i.e., frameshift) post-M135 have highest METSSs of these categories ( $n = 14$ ; median METSS 1.5). Significant difference between pre- and post-M135 nonconservative METSSs. Disruptive carriers are significantly different from every other category. Data suggest that missense variants reducing AF-1 function protect carriers from metabolic dysfunction compared with other *PPARG* missense variants. **D**: TG/HDL, a measurement for insulin resistance, is plotted by position and conservation. Pre-M135 nonconservative variant carriers have lowest median TG/HDL (-0.080). Carriers of disruptive variants have significantly higher TG/HDLs, with significant difference between pre- and post-M135 nonconservative variant carriers. \* $P = 0.016$  (C) and  $P = 0.017$  (D) by Welch t test, \*\*\* $P < 2e-16$  (B), # $P = 4.1e-6$  by ANOVA and  $P < 8.6e-4$  by Tukey HSD (C) and  $P = 7.31e-7$  by ANOVA and  $P < 1.1e-4$  by Tukey HSD (D).

domain function increase the transcriptional activity of PPAR $\gamma$ .

To quantify insulin sensitivity in these *PPARG* missense variant carriers, we computed a per-individual metabolic syndrome severity score (METSS), a measure of insulin sensitivity determined from waist circumference, SBP, serum TGs, HDL cholesterol, and serum glucose (HbA<sub>1c</sub>), using methods analogous to those previously published (41–43). We calculated METSS for the 368,911 individuals in the UK Biobank who had all five measurements ascertained, including 908 of the 1,250 carriers of rare protein-coding *PPARG* variants (Supplementary Fig. 3A and B). Of the rare *PPARG* missense variant carriers in the UK Biobank, 340 pre-M135 and 370 post-M135 carriers had computable METSS values. As with the PPAR $\gamma$  function score analysis above (Fig. 5B), we partitioned each group according to conservative and nonconservative BLOSUM62 to examine the effect of each variant category on METSS (Fig. 5C). Under the model that amino acid substitutions that abrogate AF-1 domain function would increase PPAR $\gamma$  activity and thereby decrease METSS, we hypothesized that nonconservative missense variants in AF-1 (pre-M135) would confer lower METSS as compared with conservative amino acid substitutions that would preserve AF-1 function. Conversely, we expected that nonconservative mutations post-M135 in the DBD or LBD would increase METSS, as is the case for lipodystrophy (44). As a positive control, we identified carriers of post-M135 disruptive (i.e., nonsense and frameshift causing) *PPARG* variants ( $n = 14$ ) in our cohort and found their METSS to be significantly elevated (median METSS 1.5) (Fig. 5D) compared with other *PPARG* variant carriers (ANOVA  $P = 4.1e-6$ ; Tukey  $P < 8.6e-4$ ) and the general UK Biobank population (Welch  $t$  test  $P = 1.1e-4$ ). We observed an ordinal trend, with nonconservative pre-M135 variant carriers having the lowest METSS (median METSS  $-0.079$ ), followed by conservative pre-M135 (median METSS 0.0064), conservative post-M135 (median METSS 0.24), and finally nonconservative post-M135 (median METSS 0.36) carriers. The difference between pre- and post-M135 nonconservative variant carriers was significant (Welch  $t$  test  $P = 0.016$ ).

We performed a similar analysis alternatively using the ratio of serum TGs to HDL cholesterol (TG/HDL) as a surrogate measure of insulin sensitivity (45,46). The trends observed with METSS were consistent in the TG/HDL results; carriers of post-M135 disruptive (i.e., nonsense and frameshift causing) *PPARG* variants ( $n = 15$ ) had the highest values compared with other *PPARG* variant carriers (median TG/HDL 1.65; ANOVA  $P = 7.31e-7$ ; Tukey HSD  $P < 1.1e-4$ ) (Fig. 5D), and the nonconservative pre-M135 variant carriers had the lowest TG/HDL ( $n = 108$ ; median TG/HDL  $-0.080$ ). The difference between pre- and post-M135 nonconservative variant carriers was significant (Welch  $t$  test  $P = 0.017$ ).

We separately analyzed the well-known *PPARG* p.P12A variant (rs1801282; minor allele frequency 0.1050) that is associated with decreased type 2 diabetes risk (47) and

occurs frequently in the general population. Under the above partitioning scheme, *PPARG* p.P12A would be classified as pre-M135 nonconservative (FS 1.3; BLOSUM62 score  $-1$ ). Carriers of the p.P12A allele ( $n = 80,882$ ) in the UK Biobank had significantly decreased METSS (per allele effect size  $-0.039$ ;  $P = 2e-16$ ) (Supplementary Fig. 3C and Supplementary Table 6). These data are suggestive of a model in which AF-1-disrupting variants (both common and rare) can improve insulin sensitivity in vivo.

## DISCUSSION

Here, we characterize a novel isoform of PPAR $\gamma$ , termed PPAR $\gamma$  M135, which lacks the AF-1 domain and can be generated from an alternative translational start site. In both macrophages and adipocytes, PPAR $\gamma$  M135 is transcriptionally active, ligand inducible, and more potent than WT PPAR $\gamma$ , likely because of derepression from the loss of the AF-1 domain. We also assess insulin sensitivity in human carriers of *PPARG* variants, demonstrating that variants impairing the AF-1 domain may protect carriers from insulin resistance. Our data support a model for in vivo derepression of PPAR $\gamma$  in humans that is metabolically beneficial.

Our findings that PPAR $\gamma$  M135 enhances transactivation and improves metabolic health align with studies of naturally occurring and synthetic PPAR $\gamma$  variations. Previous investigations demonstrated that deleting the PPAR $\gamma$  N-terminus increases transcriptional potency compared with WT in NIH-3T3 cells (48,49), and a MAPK phosphorylation site at PPAR $\gamma$  p.S112 inhibits PPAR $\gamma$  transactivation. PPAR $\gamma$  p.S112A, which lacks the phosphorylation site, is more transcriptionally active (50). Additionally, PPAR $\gamma$ 2 p.P12A (rs1801282), which is associated with a reduced risk of type 2 diabetes (47), weakens the interaction between PPAR $\gamma$  and its corepressor NCoR, resulting in increased expression of PPAR $\gamma$  target genes and improved insulin sensitivity in mice (51). Our data corroborate these mechanisms, because METSS decreased per p.P12A allele. Furthermore, SUMOylation at p.K107 inhibits ligand-induced transactivation of PPAR $\gamma$  targets (52), and removing that modification increases insulin sensitivity without increasing adiposity in mice (53). Together, these studies illustrate that impairing the AF-1 domain increases PPAR $\gamma$  activity and insulin sensitivity.

Regarding therapeutic development, our study proposes a new method to activate PPAR $\gamma$  distinct from TZDs, which target the LBD. We propose the AF-1 domain as a therapeutic target that is mechanistically distinct from TZDs and selective PPAR $\gamma$  modulators, because removing AF-1 would derepress rather than activate PPAR $\gamma$ . Accordingly, our data show that adipocytes engineered to produce PPAR $\gamma$  M135 expressed higher levels of adiponectin, an insulin-sensitizing adipokine (54), and had increased Akt phosphorylation in response to insulin stimulation. Further supporting this proposal are the murine models of human and synthetic *PPARG* variants that increase PPAR $\gamma$  activity via impairing AF-1

(p.P12A (51), p.S112A (55), and p.K107 (53)), showing enhanced insulin sensitivity compared with WT littermates.

Limitations of our study include the use of in vitro cell models, the number of human carriers with analyzable *PPARG* protein-coding variants, and the generalizability of the UK Biobank population. The THP-1 monocyte and SGBS preadipocyte cell lines, although human, do not fully replicate in vivo conditions; however, they have shown consistent results in prior *PPARG* variant studies (8,9,18). Furthermore, PPAR $\gamma$  is active in other tissues, including muscle and liver, which may have additional metabolic consequences (56,57). These could be the subjects of future investigations to fully dissect the metabolic consequences of PPAR $\gamma$  M135. In addition, the number of human carriers of AF-1 domain nonconservative missense variants ( $n = 94$ ) limited our statistical power to detect changes in metabolic syndrome severity in this group. Moreover, the UK Biobank represents a relatively healthy middle-aged population of largely British ancestry, which is not representative of global populations (58). In the future, our approach could be easily reapplied to larger cohorts and multiethnic samples to corroborate and strengthen our findings as they become available to investigators. Another future direction would be to validate the therapeutic hypothesis of generating PPAR $\gamma$  M135 in vivo using transgenic murine models and evaluate tissue specificity.

In summary, we present PPAR $\gamma$  M135, a novel isoform of *PPARG* arising from an alternative translational start site, as a more potent transactivator than full-length PPAR $\gamma$ . This work points to a new mechanism of activating PPAR $\gamma$  by inhibiting the AF-1 domain, which could lead to more effective treatments for insulin resistance-related disorders.

**Acknowledgments.** The authors thank the All of Us participants, because the All of Us Research Program would not be possible without their partnership. The authors are grateful to Angela Liu for technical assistance. Microscopy was performed at the Nikon Imaging Center at University of California San Diego with the support of P. Guo and R. Sanchez. This research was conducted using the UK Biobank resource under applications 41189 and 51436. The authors acknowledge the participants of and the contributions made by UK Biobank ([www.ukbiobank.ac.uk](http://www.ukbiobank.ac.uk)) in providing the data and resources used in this study.

**Funding.** This work was supported by grants 1R01DK123422 and R01HL159760 (A.R.M.) and 1R01DK125490 (J.F., A.R.M.) from the National Institute of Diabetes and Digestive and Kidney Diseases and University of California (UC) San Diego/UC Los Angeles Pilot and Feasibility grant P30 DK063491 (A.R.M.). This publication includes data generated at the UC San Diego Institute for Genomic Medicine Genomics Center using an Illumina NovaSeq 6000 that was purchased with funding from National Institutes of Health Shared Instrument grant S10 OD026929. The All of Us Research Program is supported by the Office of the Director, National Institutes of Health, through regional medical centers (grants 1 OT2 OD026549, 1 OT2 OD026554, 1 OT2 OD026557, 1 OT2 OD026556, 1 OT2 OD026550, 1 OT2 OD026552, 1 OT2 OD026553, 1 OT2 OD026548, 1 OT2 OD026551, and 1 OT2 OD026555), an interagency agreement (AOD 16037), federally qualified health centers (grant HHSN 263201600085U), a data and research center (grant 5 U2C OD023196), a biobank (grant 1 U24 OD023121), a participant center (grant U24 OD023176), a participant technology systems center (grant 1 U24 OD023163), communications and engagement (grants 3 OT2 OD023205 and 3 OT2

OD023206), and community partners (grants 1 OT2 OD025277, 3 OT2 OD025315, 1 OT2 OD025337, and 1 OT2 OD025276).

**Duality of Interest.** No potential conflicts of interest relevant to this article were reported.

**Author Contributions.** X.D., K.M.-L., S. Hu, R.D., G.B., R.H., J.F., S. He., and A.R.M. were involved in data interpretation. X.D., K.M.-L., and A.R.M. designed the experiments and drafted the initial manuscript. A.R.M. conceived the study. All authors generated/acquired and analyzed the data and were involved in manuscript revision. A.R.M. is the guarantor of this work and, as such, had full access to all the data in the study and takes responsibility for the integrity of the data and the accuracy of the data analysis.

## References

- James DE, Stöckli J, Birnbaum MJ. The aetiology and molecular landscape of insulin resistance. *Nat Rev Mol Cell Biol* 2021;22:751–771
- Yki-Järvinen H. Thiazolidinediones. *N Engl J Med* 2004;351:1106–1118
- Tontonoz P, Hu E, Graves RA, Budavari AI, Spiegelman BM. mPPAR gamma 2: tissue-specific regulator of an adipocyte enhancer. *Genes Dev* 1994;8:1224–1234
- Inzucchi SE, Viscoli CM, Young LH, et al.; IRIS Trial Investigators. Pioglitazone prevents diabetes in patients with insulin resistance and cerebrovascular disease. *Diabetes Care* 2016;39:1684–1692
- DePaoli AM, Higgins LS, Henry RR, Mantzoros C, Dunn FL; INT131-007 Study Group. Can a selective PPAR $\gamma$  modulator improve glycemic control in patients with type 2 diabetes with fewer side effects compared with pioglitazone? *Diabetes Care* 2014;37:1918–1923
- Savage DB, Tan GD, Acerini CL, et al. Human metabolic syndrome resulting from dominant-negative mutations in the nuclear receptor peroxisome proliferator-activated receptor-gamma. *Diabetes* 2003;52:910–917
- Agostini M, Schoenmakers E, Mitchell C, et al. Non-DNA binding, dominant-negative, human PPARgamma mutations cause lipodystrophic insulin resistance. *Cell Metab* 2006;4:303–311
- Majithia AR, Flannick J, Shahinian P, et al.; T2D-GENES Consortium. Rare variants in *PPARG* with decreased activity in adipocyte differentiation are associated with increased risk of type 2 diabetes. *Proc Natl Acad Sci U S A* 2014;111:13127–13132
- Majithia AR, Tsuda B, Agostini M, et al.; UK Congenital Lipodystrophy Consortium. Prospective functional classification of all possible missense variants in *PPARG*. *Nat Genet* 2016;48:1570–1575
- Jiao Y, Ahmed U, Sim MFM, et al. Discovering metabolic disease gene interactions by correlated effects on cellular morphology. *Mol Metab* 2019;24:108–119
- Heinz S, Texari L, Hayes MGB, et al. Transcription elongation can affect genome 3D structure. *Cell* 2018;174:1522–1536.e22
- Robinson MD, McCarthy DJ, Smyth GK. edgeR: a Bioconductor package for differential expression analysis of digital gene expression data. *Bioinformatics* 2010;26:139–140
- Law CW, Chen Y, Shi W, Smyth GK. voom: precision weights unlock linear model analysis tools for RNA-seq read counts. *Genome Biol* 2014;15:R29
- Conway JR, Lex A, Gehlenborg N. UpSetR: an R package for the visualization of intersecting sets and their properties. *Bioinformatics* 2017;33:2938–2940
- Korotkevich G, Sukhov V, Budin N, Shpak B, Artyomov MN, Sergushichev A. Fast gene set enrichment analysis. *bioRxiv*. 1 February 2021 [preprint]. Available from <https://www.biorxiv.org/content/10.1101/060012v3>
- Cingolani P, Platts A, Wang LL, et al. A program for annotating and predicting the effects of single nucleotide polymorphisms, SnpEff: SNPs in the genome of *Drosophila melanogaster* strain w1118; iso-2; iso-3. *Fly (Austin)* 2012;6:80–92
- Evangelou E, Warren HR, Mosen-Ansorena D, et al.; Million Veteran Program. Genetic analysis of over 1 million people identifies 535 new loci associated with blood pressure traits. *Nat Genet* 2018;50:1412–1425

18. Agostini M, Schoenmakers E, Beig J, et al. A pharmacogenetic approach to the treatment of patients with PPARG mutations. *Diabetes* 2018;67:1086–1092
19. Tontonoz P, Nagy L, Alvarez JG, Thomazy VA, Evans RM. PPARgamma promotes monocyte/macrophage differentiation and uptake of oxidized LDL. *Cell* 1998;93:241–252
20. Aryal B, Rotllan N, Araldi E, et al. ANGPTL4 deficiency in haematopoietic cells promotes monocyte expansion and atherosclerosis progression. *Nat Commun* 2016;7:12313
21. Lefterova MI, Zhang Y, Steger DJ, et al. PPARgamma and C/EBP factors orchestrate adipocyte biology via adjacent binding on a genome-wide scale. *Genes Dev* 2008;22:2941–2952
22. Hodgkinson CP, Ye S. Microarray analysis of peroxisome proliferator-activated receptor-gamma induced changes in gene expression in macrophages. *Biochem Biophys Res Commun* 2003;308:505–510
23. Gažová I, Lefevre L, Bush SJ, et al. The transcriptional network that controls growth arrest and macrophage differentiation in the human myeloid leukemia cell line THP-1. *Front Cell Dev Biol* 2020;8:498
24. Genin M, Clement F, Fattaccioli A, Raes M, Michiels C. M1 and M2 macrophages derived from THP-1 cells differentially modulate the response of cancer cells to etoposide. *BMC Cancer* 2015;15:577
25. Kim JB, Wright HM, Wright M, Spiegelman BM. ADD1/SREBP1 activates PPARgamma through the production of endogenous ligand. *Proc Natl Acad Sci U S A* 1998;95:4333–4337
26. Ma J-J, Zhang T, Fang N, et al. Establishment of a cell-based drug screening model for identifying agonists of human peroxisome proliferator-activated receptor gamma (PPAR $\gamma$ ). *J Pharm Pharmacol* 2012;64:719–726
27. Hsu HY, Nicholson AC, Hajjar DP. Inhibition of macrophage scavenger receptor activity by tumor necrosis factor-alpha is transcriptionally and post-transcriptionally regulated. *J Biol Chem* 1996;271:7767–7773
28. Rovera G, O'Brien TG, Diamond L. Induction of differentiation in human promyelocytic leukemia cells by tumor promoters. *Science* 1979;204:868–870
29. de Morrée A, Flix B, Bagaric I, et al. Dysferlin regulates cell adhesion in human monocytes. *J Biol Chem* 2013;288:14147–14157
30. Pott S, Kamrani NK, Bourque G, Pettersson S, Liu ET. PPARG binding landscapes in macrophages suggest a genome-wide contribution of PU.1 to divergent PPARG binding in human and mouse. *PLoS One* 2012;7:e48102
31. Keller MD, Notarangelo LD, Malech HL. Future of care for patients with chronic granulomatous disease: gene therapy and targeted molecular medicine. *J Pediatric Infect Dis Soc* 2018;7(Suppl. 1):S40–S44
32. Chang JT, Nevins JR. GATHER: a systems approach to interpreting genomic signatures. *Bioinformatics* 2006;22:2926–2933
33. Yu G, Wang L-G, Han Y, He Q-Y. clusterProfiler: an R package for comparing biological themes among gene clusters. *OMICS* 2012;16:284–287
34. Ashburner M, Ball CA, Blake JA, et al. Gene ontology: tool for the unification of biology. The Gene Ontology Consortium. *Nat Genet* 2000;25:25–29
35. Gene Ontology Consortium. The Gene Ontology resource: enriching a GOld mine. *Nucleic Acids Res* 2021;49:D325–D334
36. Mosure SA, Munoz-Tello P, Kuo KT, et al. Structural basis of interdomain communication in PPAR $\gamma$ . *bioRxiv*. 13 July 2022 [preprint]. Available from <https://www.biorxiv.org/content/10.1101/2022.07.13.499031v3.full>
37. Wabitsch M, Brenner RE, Melzner I, et al. Characterization of a human preadipocyte cell strain with high capacity for adipose differentiation. *Int J Obes Relat Metab Disord* 2001;25:8–15
38. Combs TP, Wagner JA, Berger J, et al. Induction of adipocyte complement-related protein of 30 kilodaltons by PPARgamma agonists: a potential mechanism of insulin sensitization. *Endocrinology* 2002;143:998–1007
39. Backman JD, Li AH, Marcketta A, et al.; DiscovEHR. Exome sequencing and analysis of 454,787 UK Biobank participants. *Nature* 2021;599:628–634
40. Henikoff S, Henikoff JG. Amino acid substitution matrices from protein blocks. *Proc Natl Acad Sci U S A* 1992;89:10915–10919
41. Gurka MJ, Lilly CL, Oliver MN, DeBoer MD. An examination of sex and racial/ethnic differences in the metabolic syndrome among adults: a confirmatory factor analysis and a resulting continuous severity score. *Metabolism* 2014;63:218–225
42. Caverro-Redondo I, Martínez-Vizcaino V, Álvarez-Bueno C, Agudo-Conde C, Lugones-Sánchez C, García-Ortiz L. Metabolic syndrome including glycated hemoglobin A<sub>1c</sub> in adults: is it time to change? *J Clin Med* 2019;8:2090
43. Agarwal S, Jacobs DR, Vaidya D, et al. Metabolic syndrome derived from principal component analysis and incident cardiovascular events: the Multi Ethnic Study of Atherosclerosis (MESA) and Health, Aging, and Body Composition (Health ABC). *Cardiol Res Pract* 2012;2012:919425
44. Jeninga EH, Gurnell M, Kalkhoven E. Functional implications of genetic variation in human PPARgamma. *Trends Endocrinol Metab* 2009;20:380–387
45. Oliveri A, Rebernick RJ, Kuppa A, et al. Comprehensive genetic study of the insulin resistance marker TG:HDL-C in the UK Biobank. *Nat Genet* 2024;56:212–221
46. DeForest N, Wang Y, Zhu Z, et al. Genome-wide discovery and integrative genomic characterization of insulin resistance loci using serum triglycerides to HDL-cholesterol ratio as a proxy. *Nat Commun* 2024;15:8068
47. Altshuler D, Hirschhorn JN, Klannemark M, et al. The common PPARgamma Pro12Ala polymorphism is associated with decreased risk of type 2 diabetes. *Nat Genet* 2000;26:76–80
48. Tontonoz P, Hu E, Spiegelman BM. Stimulation of adipogenesis in fibroblasts by PPAR gamma 2, a lipid-activated transcription factor. *Cell* 1994;79:1147–1156
49. Hummasti S, Tontonoz P. The peroxisome proliferator-activated receptor N-terminal domain controls isotype-selective gene expression and adipogenesis. *Mol Endocrinol* 2006;20:1261–1275
50. Adams M, Reginato MJ, Shao D, Lazar MA, Chatterjee VK. Transcriptional activation by peroxisome proliferator-activated receptor gamma is inhibited by phosphorylation at a consensus mitogen-activated protein kinase site. *J Biol Chem* 1997;272:5128–5132
51. Heikkinen S, Argmann C, Feige JN, et al. The Pro12Ala PPARgamma2 variant determines metabolism at the gene-environment interface. *Cell Metab* 2009;9:88–98
52. Pascual G, Fong AL, Ogawa S, et al. A SUMOylation-dependent pathway mediates transrepression of inflammatory response genes by PPAR-gamma. *Nature* 2005;437:759–763
53. Katafuchi T, Holland WL, Kollipara RK, Kittler R, Mangelsdorf DJ, Kliewer SA. PPAR $\gamma$ -K107 SUMOylation regulates insulin sensitivity but not adiposity in mice. *Proc Natl Acad Sci U S A* 2018;115:12102–12111
54. Stern JH, Rutkowski JM, Scherer PE. Adiponectin, leptin, and fatty acids in the maintenance of metabolic homeostasis through adipose tissue crosstalk. *Cell Metab* 2016;23:770–784
55. Rangwala SM, Rhoades B, Shapiro JS, et al. Genetic modulation of PPARgamma phosphorylation regulates insulin sensitivity. *Dev Cell* 2003;5:657–663
56. Norris AW, Chen L, Fisher SJ, et al. Muscle-specific PPARgamma-deficient mice develop increased adiposity and insulin resistance but respond to thiazolidinediones. *J Clin Invest* 2003;112:608–618
57. Gavrilova O, Haluzik M, Matsusue K, et al. Liver peroxisome proliferator-activated receptor gamma contributes to hepatic steatosis, triglyceride clearance, and regulation of body fat mass. *J Biol Chem* 2003;278:34268–34276
58. Fry A, Littlejohns TJ, Sudlow C, et al. Comparison of sociodemographic and health-related characteristics of UK Biobank participants with those of the general population. *Am J Epidemiol* 2017;186:1026–1034